
# The Potential adaptation of stationary shoulder friction stir welding technology to steel

Charles A. Maltin, Lauren J. Nolton, Jamie L. Scott, Athanasios I. Toumpis, Alexander M. Galloway

PII: S0261-3069(14)00633-5
DOI: http://dx.doi.org/10.1016/j.matdes.2014.08.017
Reference: JMAD 6714

To appear in: *Materials and Design*

Received Date: 11 May 2014
Accepted Date: 7 August 2014

Please cite this article as: Maltin, C.A., Nolton, L.J., Scott, J.L., Toumpis, A.I., Galloway, A.M., The Potential adaptation of stationary shoulder friction stir welding technology to steel, *Materials and Design* (2014), doi: http://dx.doi.org/10.1016/j.matdes.2014.08.017

# THE POTENTIAL ADAPTATION OF STATIONARY SHOULDER FRICTION STIR WELDING TECHNOLOGY TO STEEL

**CHARLES A MALTIN*, LAUREN J NOLTON, JAMIE L SCOTT, ATHANASIOS I TOUMPIS, ALEXANDER M GALLOWAY**

*Mechanical and Aerospace Engineering, Mechanical and Aerospace Engineering, Level 8, James Weir Building, 75 Montrose Street, Glasgow, G1 1XJ.*

**Corresponding author; Email: charles.maltin@strath.ac.uk ; Tel: +447557224982*

## Abstract

Stationary shoulder friction stir welding is a newly developed technique currently used for joining plates of relatively soft metals at different angular planes. The process is not currently applicable to steel, hence the present study was developed to investigate the theoretical and technical viability of stationary shoulder technology in DH36 steel. Aluminium welds were produced using both conventional rotating shoulder and stationary shoulder friction stir welding techniques, and steel welds were produced using only conventional friction stir welding techniques. The effects of stationary shoulder technology on both the microstructural evolution and resultant mechanical properties of aluminium have been evaluated so that the likely effects on steel could be predicted. In the aluminium welds, the stationary shoulder technique results in a distinct transition between stirred and unstirred material, contrasting to the gradual change typically seen in conventional friction stir welds produced with a rotating shoulder. An investigation of weld properties produced in DH36 steel has demonstrated that if the stationary shoulder weld technique was used, the microstructure likely to be formed, would be dominated by a bainitic ferrite phase and so would exhibit hardness and tensile properties in excess of the parent material. It is predicted that if the same abrupt transition between unstirred and stirred material observed in aluminium occurred in steel, this would lead to crack initiation, followed by rapid propagation through the relatively brittle weld microstructure. Hence, these findings demonstrate that without further design and process improvements, stationary shoulder friction stir welding is unlikely to be applicable to steel.

***Keywords***

*Friction Stir Welding; Low Alloy Steel; Stationary Shoulder*

## 1. Introduction

Friction stir welding (FSW) is a solid state joining process that develops a localised thermo-mechanically affected zone in the weld region [1]. The basic FSW process involves a specially designed, non-consumable, rotating cylindrical tool comprising a shoulder and a protruding pin that is of a length typically just less than the thickness to be welded [1-3]. The rotating tool is plunged downwards into the joint before being traversed along it. During the plunging phase of the process, the material is plasticised as a result of frictional heat generation [2]. However, temperatures are always maintained below the melting point, hence the solid state nature of the process [4]. The localised heating is facilitated in two ways; firstly as a result of friction between the rotating shoulder and the face of the work piece; and secondly, due to the visco-plastic dissipation of mechanical energy within the material [1, 2, 5]. As a result of the rotation and translation of the tool, the plasticised material is moved around it, from front to back, before being locally forged to form the welded joint [1-3].

The initial development of FSW focused on aluminium alloys, in particular those considered problematic when joined by conventional fusion welding processes [1, 2]. In such alloys, the solid state nature of FSW leads to a number of benefits in terms of the mechanical and metallurgical properties of the resultant joint. For example, since there is no melting of material, the issues typically associated with solidification do not present a problem [1]. There cannot be solidification cracking, nor elemental segregation, hence the formation of brittle phases due to terminal eutectic type reactions does not occur. Since there is no molten weld pool, porosity due to gas trapped within it cannot occur [5]. In addition to the absence of these defects typically associated with fusion welding processes, friction stir welds have been documented to have excellent mechanical properties as well as demonstrating low levels of distortion and residual stress [1, 5].

As the benefits of FSW have been reported, the technique has found application in various industries using a variety of different materials [5], including extensive use in the aerospace industry where the joining of light alloys which derive their mechanical properties from the precipitation of strengthening particles is crucial [6]. It is only in very recent years that this technology has been adapted to perhaps one of the most promising applications – the FSW of carbon and stainless steels [4]. FSW of steels has only been recently realised primarily as a result of issues in tooling material selection and development. The tool must exhibit high strength, wear resistance, fracture toughness and a resistance to chemical degradation all at the high temperatures associated with FSW [7-9]. Hence, finding a material which meets all of these requirements whilst producing industrially useful weld lengths has proved to be a significant engineering challenge, with studies being carried out into various ceramic options [7]. However, composite poly-crystalline Boron Nitride/Tungsten-Rhenium (pcBN/W-Re) tools are now becoming commercially available and facilitate FSW of steels [4].

FSW has found extensive use in the aerospace industry, where T-joints are a common geometry and are employed for the attachment of a structural stiffener to the main panel [6, 10]. Both Fratini *et al*. [6] and Acerra *et al.* [10] utilised FSW technology to manufacture such a T-joint. This involved the pin of the FSW tool penetrating through the thickness of the skin and into the stringer. In addition, a specialised die was required to provide the localised forging of the plasticised material and hence the desired fillet radius. In both cases, the importance of the process parameters (tool rotation and traverse speed) were noted and macroscopic defects such as tunnelling were seen in the instances where these parameters were outside of optimum [6, 10]. Furthermore, Acerra *et al*. [10] observed deleterious effects attributed to the coating applied to the materials. Moreover, Fratinit *et al*. [6] conducted bend tests and deemed the behaviour to be unsatisfactory with cracking evident at "*very low values of bending angle*" [6].

Recent developments in FSW tooling technology may provide an alternative method for producing such T-joints. As reported by Martin *et al.* [11], the use of a shaped stationary shoulder allows for the joining of plates which are at different angular planes and schematics of both conventional rotating shoulder and stationary shoulder techniques are shown in Figures 1(a) and 1(b). This methodology does not result in the undercutting of the skin as reported by Acerra *et al.* [10]. As the shaped shoulder provides the localised forging of the plasticised material, it is reasonable to conclude that defects such as the ligaments noted by Steel *et al.* [12] are unlikely to be present. Stationary shoulder friction stir welding (SSFSW) does not inherently provide a fillet radius in a T-joint and thus from a loading perspective, the joint may be subject to significant stress concentration. Therefore, as reported by Martin *et al.* [11], a filler wire may be incorporated into the joint by forcing this additional plasticised material into the weld. However, there is no published research outside of that presented by Martin *et al.* [11] into the mechanical properties of the weld produced using SSFSW technology.

There is significant demand to adapt the FSW technology to carbon and stainless steels and it is therefore envisaged that there will soon be an increasing requirement for producing T-joints in steels. As discussed by Steel *et al.* [12], the shipbuilding industry would find significant application for such advancement in the attachment of longitudinal stiffeners to plate, where low distortion and minimal re-working is key and hence the FSW process would be ideally suited.

The adaption of SSFSW technology to steel has not yet been achieved and its realisation is likely to be highly dependent upon the development of a tool capable of facilitating such a weld. Tool material selection for higher plasticisation temperature metals has been the subject of previous studies [4, 9] and initially tool materials were categorised into either refractory metals (such as W-Re) or super abrasive tools (such as pcBN) [9]. In recent developments, manufacturers have combined these in the form of composite pcBN-WRe tools.

The problem envisaged for SSFSW of these higher temperature plasticisation materials (ferrous and nickel based alloys) is that without the presence of a shoulder, tool rotation speed will need to be higher in order to generate the same frictional heating that is required to sufficiently plasticise the material. It is predicted that this higher rotational speed will lead to increased wear and failure rates even in the pcBN-WRe tools. Hence, as discussed by Sorensen *et al.* [9] in the development of early W based tools, preheating of the tool or initial pilot hole drilling may be required.

If SSFSW is to be achieved for steel, and assuming that a tool capable of producing such a weld could be developed, it is important that the microstructural evolution and hence mechanical properties of the resultant weld are predicted and understood.

The aim of the present investigation is to determine if the transfer of SSFSW technology to steel would be technically viable, and to assess what would be the likely metallurgical features and hence mechanical properties resulting from the application of SSFSW to steel. In order to assess the transfer of stationary shoulder technology to steel, it was necessary to determine the characteristic effect of the process when applied to aluminium, and hence the likely microstructural evolution which may occur if the same technique was used in steel.

## 2. Experimental Methods

### *2.1. Friction Stir Butt Welding of Steel*

Conventional rotating shoulder friction stir welds were produced in 6mm thick DH36 grade steel, with the welding direction perpendicular to the plate rolling direction. A MegaStir Q70 tool (36.8mm scrolled shoulder with stepped spiral probe of length 5.7mm with a composition of 70% pcBN/30% W-Re) was utilised within a shielding argon gas atmosphere in order to protect the tool surface: similar techniques were documented by Cater *et al.* [4]. The welding procedure used a zero degree tool tilt and employed no preheating of the tool or the plates to be welded. A PowerStir FSW machine (capable of max. torque 2480Nm and max. down force 150kN) was used in position control in order to maintain constant distance from a given datum point irrespective of the forces acting upon the welding head. The nominal composition of the DH36 grade steel is provided in Table 1.

A standard square edge butt weld configuration was used. As it was also of interest to evaluate the effect of parameter variation on the obtained microstructure and properties, four different sets of parameters were utilised. These parameters are provided in Table 2. Three of the welds (W1, W2 and W3) were produced with the same tool rotation speed and slight variations in traverse speed whilst the fourth weld (W4) employed significantly different parameters with high rotational speed and high traverse speed. All steel friction stir welds were produced over a total length of 300mm.

### *2.2. Friction Stir Welding of Aluminium Butt and T Joints*

Conventional rotating shoulder friction stir welds were produced in 6mm thick 6082-T6 aluminium in a direction perpendicular to the rolling direction of the plate. The welds were made in standard square edge butt weld configuration for a total length of 500mm and an overall width of 250mm. The parameters were maintained as constant upon reaching the steady state at 600rpm rotational speed and 600mm/min traverse speed. The nominal composition of the 6082-T6 aluminium is provided in Table 3, [5].

SSFSW with the addition of filler wire [11] in a T joint configuration (base 100mm wide; leg 75mm tall), were produced in 8mm thick 6082-T6 aluminium over a total length of 350mm. The welding parameters were maintained as constant over the steady state region of the weld at 1200rpm and 200mm/min for the first side of the T joint and 1200rpm and 120mm/min for the second side.

All aluminium welds were produced using a Manufacturing Technology Incorporated (MTI) precision spindle FSW machine capable of a maximum torque of 350Nm and a maximum down force of 100kN.

### *2.3. Mechanical Testing of Aluminium and Steel Butt Welds*

All friction stir butt welds were subjected to a series of mechanical testing in accordance with ASTM: A370.

Standard size transverse tensile specimens were extracted from the aluminium plate with a gauge length of 50mm. Specimens were machined from different locations on the plate in order to evaluate if the location within the weld would affect the site or mode of failure. All tensile testing of the aluminium was conducted using an INSTRON 8802 Servohydraulic tensile testing system with a maximum capacity of 250kN and a cross-head speed of 1mm/min. Sub size Charpy V-notch specimens (5x10x55mm) were also machined from the aluminium plate and notched through the face of the weld and in the centreline.

The steel friction stir welds were all subject to the same mechanical testing regime. Sub size all weld metal tensile (AWMT) specimens were extracted longitudinally, of 25mm gauge length and machined from identical locations in each of the 4 plates. In addition, sub size transverse tensile and parent material tensile specimens, of 25mm gauge length, were also tested. Due to the steel tensile specimens being sub size, an INSTRON 5969 Electromechanical tensile testing system was utilised with a cross-head speed of 0.5mm/min to 4% strain followed by 2mm/min thereafter. Sub size Charpy V-notch specimens (5x10x55mm) were extracted and notched in the weld metal centreline.

All Charpy V-notch testing was conducted using a standard pendulum with a maximum energy of 294.2J.

### *2.4. Mechanical Testing of Aluminium T-Joints*

The stationary shoulder friction stir T-joint welds in aluminium were tested using T pull off, pull apart and bend tests. The pull off test involved gripping the base of the T section and applying tensile load to the leg, whereas the pull apart test applied uniaxial tensile load across the base of the T. For both pull off and pull apart tests, an INSTRON 8802 Servohydraulic tensile testing system was used. The bend tests utilised within the present study involved machining the T section such that half of the base was removed and the leg was of equal length as shown in Figure 2. The specimen was then crushed until flat, thus subjecting the face of the weld to tensile bending stress.

### *2.5. Microstructural Characterisation*

All specimens had macro sections removed from the weld and were subjected to a grinding and polishing sequence to a final abrasive particle size of 0.05μm colloidal silica using a Struers Rotopol-22 with a Rotoforce 4 head. Microhardness mapping was conducted using a Mitutoyo microhardness tester with a 200g load and a grid spacing of 1mm. Mapping was carried out on all of the friction stir welded steel specimens. Microhardness mapping was also carried out on both the butt and T-joints made in aluminium. A 1mm grid was utilised in order to characterise the entire weld section; this resulted in a 31x5mm grid for the butt section and a 7x16mm grid for the T-joint.

All light optical microscopy (LOM) was carried out using an Olympus GX51 microscope with polarising lens and differential interference contrast (DIC) capabilities. LOM was conducted in a systematic manner with specific regions of the weld sections being imaged in order to characterise the entire weld area whilst maintaining an objective approach.

Aluminium specimens were etched using Keller's reagent whereas all steel specimens were etched using 5% nital (5% nitric acid; 95% ethanol).

## 3. Results and Discussion

### *3.1. Steel Microstructural Characterisation*

Macro sections were extracted and prepared from the friction stir steel welds designated W1, W2, W3 and W4 and the corresponding macrographs are provided in Figures 3(a), 3(b), 3(c), and 3(d) respectively with the advancing side of the weld shown on the left in all cases.

Considering the first three welds where the rotational speed was maintained as constant and the traverse speed was incrementally increased, the parameter variation effects may be observed. The heat affected zone (HAZ) region becomes progressively narrower as the traverse speed is increased (Figure 3). The variation is most apparent when considering the change from W2 to W3 (Figures 3(b) and 3(c) respectively) where a much narrower HAZ is evident in W3. This is particularly noticeable on the advancing side of the weld in W3 where the HAZ outside of the thermo-mechanically affected zone (TMAZ) is considerably reduced. This is indicative of an increasing traverse speed leading to a higher cooling rate and thus a less gradual transition in material properties from stirred to unstirred material.

LOM of the steel microstructures was conducted in nine specific regions as shown in Figure 4 and using magnifications varying between 50x, 200x and 500x.

In all four of the steel welds investigated, there is a significant variation of resultant microstructure through the thickness of the section i.e. from the top surface to the bottom surface. This is exemplified in Figures 5(a), 5(b), and 5(c) taken from W2 in the locations of Figure 4 denoted as 2, 5 and 8 respectively, and this is observed consistently in all 4 of the welds examined. There is a transitional type behaviour in the microstructural evolution through the weld thickness.

At the surface region (location 2) as shown in Figure 5(a), the predominant phase is acicular ferrite. This is intermixed with a substantial volume fraction of bainitic ferrite as observed in the micrograph. This is in contrast to the microstructure present in Figure 5(b) (location 5) where the predominant phase is acicular ferrite but with a substantially lower constituent of the bainitic ferrite phase, and a small volume fraction of fine grained ferrite. In Figure 5(c) (location 8), the microstructure is vastly different with no regions of acicular nor bainitic ferrite present. Instead, Figure 5(c) demonstrates a very fine grained ferritic microstructure with equiaxed grains characteristic of dynamically recrystallized ferrite [13].

Although demonstrating similar transitional behaviour through the thickness of the weld, W4 has a significantly different microstructure relative to the other 3 welds. In W4, the dominant phase in the weld metal is the bainitic ferrite previously observed as a volume fraction at the surface of the other welds. This is demonstrated in the micrograph presented in Figure 6 taken from location 5 in Figure 4.

In addition, LOM substantiates the HAZ observations of the advancing side made previously when investigating the macrographs. The variation in the width of the HAZ with differing welding parameters is significantly more discernible when imaged at 50x magnification as provided in Figures 7(a), 7(b),

and 7(c) for welds W1, W2 and W3 respectively. Figure 7(a) demonstrates the extent of the HAZ in W1 and its gradual transition to parent material, this is seen to be reduced to a minor extent in Figure 7(b) and vastly narrowed in 7(c).

A feature specific to the advancing side of the weld is consistently seen in all of the steel specimens examined using LOM and to some extent when investigating the macrographs discussed previously. The root of the weld exhibits a 'swept up' type feature as evidenced by Figure 8. It is therefore suggested in the present study that this is characteristic of a friction stir weld in steel and is the result of plasticised material in the weld region being stirred from the advancing side, around the periphery of the tool's pin, to the retreating side of the weld. It is noteworthy in the present study since it demonstrates the flow of plasticised material which occurs when a rotating shouldered tool is used for the FSW of steel.

In W3, the centreline segregation within the parent material plate was observed to be stirred into the weld during the FSW process. This resulted in the swirling patterns in Figure 9. Based upon the nature of the swirling and the location within the weld metal, it is reasonable to conclude that the resultant morphology of this centreline segregation is due to the geometry of the FSW tool and more specifically the threading on the pin.

The microhardness mapping results for W1, W2, W3, and W4 steel butt welds are presented in Figures 10(a), 10(b), 10(c), and 10(d) respectively.

There is consistent hardening in the region of the weld and a less significant hardening effect in the HAZ region of the welds. The peak hardness varies only to a small extent among the specimens welded using the same rotational speed, with values of 328HV, 313HV and 322HV for W1, W2 and W3 respectively. However, there is a significant difference in peak hardness in W4 with a maximum value of 433HV being recorded. Furthermore, W4 is substantially harder in all areas of the material affected by the welding process.

In addition, the microhardness measurements also serve to demonstrate the asymmetry between advancing and retreating side of the weld – inherent to the process.

### *3.2. Aluminium Microstructural Characterisation*

Macro sections were removed and prepared from both the 6082-T6 aluminium butt welded plate and stationary shoulder T-joint, for which macrographs are provided in Figures 11(a) and 11(b).

Aside from the obvious geometrical differences of these two welds, the effect of employing the stationary shoulder technology is immediately apparent. Firstly, there are significant swirling patterns evident in the weld region of the T-joint – again these are likely associated with the threading on the pin of the FSW tool. Secondly and when considering the butt joint, the various regions typically associated with FSW are identifiable (weld nugget, TMAZ and HAZ). This may be attributed to the effect of the tool shoulder resulting in a gradual transition in the level of plastic deformation of the material and a steady dissipation of heat. In contrast, the stationary shoulder friction stir weld shows a very distinct boundary between stirred and unstirred material with minimal microstructural modification

to the material outside of the pin penetration region. A HAZ similar to that of the butt weld cannot be identified at the macroscopic level in the stationary shoulder friction stir weld.

LOM of the aluminium specimens was also conducted in specific regions in order to characterise the entirety of the welded area. The regions imaged in both the butt and T-joints are provided in Figures 12(a) and 12(b).

In comparing the microstructures of the two specimens, the initial observations made when investigating the macrographs are confirmed. It is immediately apparent that the transition between welded material and parent material is significantly more abrupt in the stationary shoulder T joint as evidenced by the micrographs of location 3 of the butt and T-joints in Figures 13(a) and 13(b) respectively.

In the butt weld, the gradual transition is seen as a progressive change in the visible particulate features and their directionality. Whereas in the T-joint, the joining line is particularly visible, with a stark change between the material affected by the welding process and that which is not. The gradual change of Figure 13(a) may not be immediately apparent and therefore serves to further demonstrate the severity of the transition between stirred and unstirred material which is the result of the SSFSW process as seen in Figure 13(b). In Figure 13(b), there are regions unaffected by the etchant and with mixing evident – the cause of these remains unclear at this stage although they are not present within the butt weld and it is therefore postulated that they are the result of the addition of a filler metal in the process.

In addition, the swirling patterns seen in the macrograph as provided in Figure 11(b) become evident when investigated at location 6 of Figure 12(b) using LOM, as shown in Figure 14.

It is interesting to note that this micrograph is captured using polarising light and DIC, which enhances any topography present within the microstructure. There is some degree of topography associated with the swirling patterns and this acts to further substantiate the theory that these are the result of threading on the pin. There are significantly fewer of these types of features in the butt weld, however upon LOM investigation similar swirling appears. As exhibited in Figure 15 (location 7 of Figure 12(a)) a similar circular pattern is noted in the lower section of the weld metal.

It is also reasonable to determine that there are two different types of features here: that which is similar to the observations made in the T-joint; and that which is darker in appearance with a less circular morphology. The darker stringer shown on the right hand side of the micrograph provided in Figure 15 may be traced from the cap of the weld to the root and is thus suggested to be a surface oxide or contaminant swept through the weld.

Figures 16(a) and 16(b) present the aluminium microhardness mapping results for the butt and T-joints respectively.

The differences in the effect of distinct FSW processes on hardness are recognisable. Considering the butt joint first as presented in Figure 16(a), the softening effect of the FSW process is noted with the prevailing minimum, i.e. excluding anomalous 'soft spots' in the region of 75HV. This is to be expected with 6082 aluminium in the T6 condition and has been well documented within the relevant literature [5, 14, 16]. Moreover, the HAZ is very broad and extends essentially to the edges of the mapped region. In addition, the hardness variation exhibits a gradual behaviour as it transitions between TMAZ and HAZ. This is in contrast to the hardness map of the T-joint as presented in Figure 16(b) where there is significantly more definition in the distinct zones of stirred material and HAZ. Although the HAZ is more significantly softened with a prevailing minimum in the region of 70HV, the stirred material (equivalent to the weld nugget in the butt weld) has a higher hardness than that in the butt weld. As previously noted, there is very little transitional behaviour moving from the stirred material to the HAZ with very well defined edges being highlighted by the microhardness mapping.

### *3.3. Steel Butt Weld Mechanical Testing*

The DH36 steel was subjected to a series of tensile and Charpy V-notch mechanical testing. Since all weld tensile tests were conducted, parent material specimens were also tested in order to determine the increase in yield strength as a result of the FSW process. The results are presented in Table 4 for yield strength (0.2% Proof Stress) and ultimate tensile stress (UTS).

All of the transverse tensile specimens fractured outside of the weld metal and exhibited very similar values of yield and ultimate strength to the parent material. The all weld metal tensile results demonstrate significant increase in both yield and ultimate stress over the parent material; the stress strain curves for all four welds are provided in Figure 17.

Clearly, the processing parameters used have very substantial effects upon the mechanical properties achieved. Among those where the rotational speed was maintained as constant and the traverse speed was varied, the highest yield strength was achieved by W2 whilst the highest UTS was recorded in W1. It is also important to consider the elongation to fracture, with W2 exhibiting strain up to 20% before fracture occurred, whereas W1 fractures just after 6% strain is achieved. The highest strengths both yield and ultimate were recorded in W4, however this weld also demonstrated the lowest elongation, fracturing at 5.57% strain.

The results of the Charpy V-notch impact testing for W1, W2, W3 and W4 (all notched in the weld metal centreline) are presented in Table 5.

It is clear that the impact toughness of the welds is relatively consistent where the rotational speed was maintained as a constant, with the highest value being recorded in W1. In contrast, there is a considerable decrease in impact toughness of W4 with an average impact energy of 38.17J being absorbed by the sub-sized specimens. This is consistent with the low strain to fracture values recorded in the tensile tests. In order to allow for comparison with steel Charpy V-notch specimens of other dimensions, the parameter $\rho$ has been calculated as used in other friction stir welding studies [16].

$$\rho = \frac{Energy\ Absorbed}{Area\ behind\ notch}\left[\frac{J}{cm^2}\right] \quad (1)$$

### 3.4. Aluminium Butt Weld Mechanical Testing

The results of the aluminium transverse tensile specimens taken from the two plate locations are provided in Table 6.

It should be noted that the specimens fractured in identical locations and with the same fracture modes – in the HAZ on the advancing side at an approximately 45° plane. Furthermore, the yield and ultimate tensile stress achieved are significantly lower than would be expected for 6082-T6 material. Typically, a 6082-T6 aluminium should achieve yield and tensile strength of 255MPa and 300MPa respectively [17]. However, the transverse tensile test results reported values approximately 100MPa less for yield strength and 50MPa less for UTS. This corresponds with the softening effect observed in the HAZ during microhardness mapping. Similar results were found by Svensson *et al.* [16] and Adamoski *et al.* [18], and such effects are attributed to the dissolution of strengthening precipitates during the FSW process followed by an insufficient time at elevated temperature for aging to be facilitated [15].

The results for the aluminium Charpy V-notch impact specimens, notched in the weld centreline, are presented in Table 7.

The impact toughness is very consistent with the 3 specimens producing results within a scatter of 1.5 Joules. Again, the parameter $\rho$ has also been presented and is compared to the Charpy V-notch impact toughness of friction stir welded 6082-T6 aluminium recorded by Janjic *et al.* [16]. In this prior study, a maximum $\rho$ value of 66.66 J/cm$^2$ was recorded in the weld metal centreline and thus is somewhat higher than the 52.08 J/cm$^2$ recorded within the present study. However, differences in $\rho$ value may be attributed to variation in the process parameters (tool rotation and traverse speed) utilised.

### 3.5. Aluminium T-Joint Mechanical Testing

The aluminium stationary shoulder T-joints were subjected to T pull and pull apart tests and the results are presented in the load extension plots of Figure 18.

Variable elongation is observed, and all specimens fractured at approximately the same value of maximum load. Furthermore, the location of fracture was consistently noted to be in the HAZ in both pull off and pull apart tests. The maximum load allows for the stress at fracture to be determined: for the pull off test, this was recorded as 268.09MPa and for the pull apart tests 1 and 2, it was found to be 273.10MPa and 268.56MPa respectively. These results are somewhat higher than the values recorded in the transverse tensile test specimens extracted from the butt weld. Moreover, in both pull apart specimens the location of fracture was on the same side; this was also the side in which fracture initiated during the pull off test. This side may be observed as the right hand weld of the macrograph in Figure 11(b) and it was therefore the second weld to be completed on these T-joints using the stationary shoulder technique.

As previously noted, the T-joints were also subjected to bend tests in which a crushing load was applied such that the face of the weld was put into tensile bending stress. A typical result is shown in Figure 19 where 3 cracks are evident on the face of the weld, two of which correspond to the interface between stirred material and the HAZ and one within the stirred material.

However, these cracks are minor considering the loading applied, and clearly demonstrate a significantly improved performance in comparison to the studies conducted by Fratini *et al.* [6] where rapid and severe crack propagation was observed at low bending strain.

### 3.6. Adaptation of SSFSW from Aluminium to Steel

The ability provided by SSFSW to join materials at different angular planes has opened considerable opportunities for industry. However, the lack of appropriate tools to facilitate this in steel presents a significant barrier to further development. The present study has explored the effect of SSFSW on 6XXX series aluminium by comparing the microstructural evolution and mechanical properties between welds produced using conventional rotating shoulder tools and SSFSW technology. Based upon these results and in conjunction with an examination of butt welds produced in steel using processing parameters attempting to replicate the thermal conditions induced in SSFSW, the viability of the technology transfer to steel has been investigated. This work is highly novel and no previous studies have been carried out elsewhere.

The data and observations presented in this study indicate that the use of a stationary shoulder as opposed to a conventional rotating shoulder tool has had significant effects on the microstructural properties of the 6082-T6 aluminium. Two key findings have provided considerable evidence to support the view that the SSFSW technique has led to a vastly elevated cooling rate of the weld and the HAZ and thus to a steep temperature gradient across stirred and unstirred material.

Firstly and for the butt and T-joint welds presented in Figures 11(a) and 11(b) respectively, there is a significant reduction in the HAZ of the T-joint. This is further substantiated by the micrographs provided for the butt and T-joints in Figures 13(a) and 13(b) respectively, where the distinct transition between stirred and unstirred material is observed in the SSFSW and is a stark comparison to the gradual variation between parent material, HAZ and TMAZ in the butt weld.

Secondly, the micro-hardness mapping revealed an extremely wide region affected by the FSW process in the butt joint (Figure 16(a)) and a much narrower area in the stationary shoulder joint. The transition between the stirred material and softened regions in the SSFSW was well defined with the mapping demonstrating a good correlation between the tool location and the hardness variation.

To understand the effect of such a temperature gradient if a stationary shoulder friction stir weld could be produced in steel, it is first necessary to evaluate the process parameters that would be required to cause plasticisation. Due to the reduced area for frictional heat generation inherent in SSFSW, it is reasonable to assume that a higher tool rotational speed would be required. In conjunction with the elevated cooling rate associated with T-joints [19], this would likely produce a weld microstructure similar to that of W4 where a high tool rotational speed was employed and a relatively high cooling

rate was produced by the higher traverse speed. Hence, this would indicate that a predominant volume fraction of the bainitic ferrite phase would be present. Mechanical testing of such a microstructure within the present investigation revealed a significant hardening effect with associated increase in both yield and tensile strength.

It is therefore predicted with considerable certainty that a similarly defined transition to that observed in the SSFSW would result in stirred and unstirred materials with vastly different mechanical properties joining abruptly. It is proposed that such a joint would lead to fracture initiating at this boundary, where the relatively brittle microstructure, as substantiated by the Charpy impact testing, would facilitate crack initiation, propagation and ultimately, failure.

This contention is further supported by Toumpis *et al.* [20] where two friction stir butt welds in DH36 steel produced using high rotational speed combined with a rapid cooling rate (due to fast traverse speed) led to fracture occurring in a brittle manner at the outer boundary of the TMAZ.

## 4. Conclusions

The aim of the present study was to investigate the feasibility of transferring SSFSW technology to DH36 steel. The data acquired and the observations made provide evidence to substantiate the view that without significant design and process improvements, satisfactory weld quality will not be achieved in steel using SSFSW. As a result of the abrupt transition between the stirred and unstirred material, failure would occur along this boundary due to the significant disparity in mechanical properties between adjacent materials, facilitating the initiation of a crack during tensile loading. Furthermore and on account of the likely processing parameters and cooling rates associated with such a weld, a relatively brittle microstructure would result through which rapid crack propagation would be facilitated.

Thus, even if appropriate tool technology is developed, SSFSW for steel may not become a practical reality due to the challenges of overcoming the microstructural and mechanical properties of such welds.

**Acknowledgements**

This work was supported by the Friction and Forge Processes Department of the Joining Technologies Group at TWI Technology Centre Yorkshire.

The authors gratefully acknowledge the financial support of the European Union which has funded this work as part of the Collaborative Research Project HILDA (High Integrity Low Distortion Assembly) through the Seventh Framework Programme (SCP2-GA-2012-314534-HILDA).

**References**

[1] Lienert T, Stellwag W, Grimmett B, Warke R. Friction stir welding studies on mild steel. Weld J Res Suppl 2003:1–9.

[2] Mishra RS, Ma ZY. Friction stir welding and processing. Mater Sci Eng R Reports 2005;50:1–78.

[3] Scialpi A, De Filippis LAC, Cavaliere P. Influence of shoulder geometry on microstructure and mechanical properties of friction stir welded 6082 aluminium alloy. Mater Des 2007;28:1124–9.

[4] Cater S, Martin J, Galloway A, McPherson N. Comparison between friction stir and submerged arc welding applied to joining DH36 and E36 shipbuilding steel. In: Mishra R, Mahoney MW, Sato Y, Hovanski Y, Verma R, editors. Friction Stir Welding and Processing VII, New Jersey: Wiley; 2013, p. 49–58.

[5] Moreira PMGP, Santos T, Tavares SMO, Richter-Trummer V, Vilaça P, de Castro PMST. Mechanical and metallurgical characterization of friction stir welding joints of AA6061-T6 with AA6082-T6. Mater Des 2009;30:180–7.

[6] Fratini L, Micari F, Squillace A, Giorleo G. Experimental Characterization of FSW T-Joints of Light Alloys. Key Eng Mater 2007;344:751–8.

[7] Perrett J, Martin J, Peterson J, Steel R, Packer S. Friction Stir Welding of Industrial Steels. In: Mishra R, Mahoney MW, Sato Y, Hovanski Y, Verma R, editors. Friction Stir Welding and Processing VI, New Jersey: Wiley; 2011, p. 65–72.

[8] Reynolds AP, Tang W, Posada M, Deloach J. Friction stir welding of DH36 steel. Sci Technol Weld Join 2003;8:455–60.

[9] Sorensen C, Nelson T. Friction stir welding of ferrous and nickel alloys. In: Mishra R, Mahoney M, editors. Friction Stir Welding and Processing, Materials Park, OH: ASM International; 2007, p. 111–21.

[10] Acerra F, Buffa G, Fratini L, Troiano G. On the FSW of AA2024-T4 and AA7075-T6 T-joints: an industrial case study. Int J Adv Manuf Technol 2009;48:1149–57.

[11] Martin J, Stanhope C, Gascoyne S. Novel techniques for corner joints using friction stir welding. In: Mishra R, Mahoney MW, Sato Y, Hovanski Y, Verma R, editors. Friction Stir Welding and Processing VI, New Jersey: Wiley; 2011, p. 179–86.

[12] Steel R, Nelson T, Sorensen C, Packer S. Friction stir welding of steel T-joint configurations. Proc. Fifteenth Int. Offshore Polar Eng. Conf., Seoul, Korea: 2005.

[13] Longfei L, Wangyue Y, Zuqing S. Dynamic recrystallization of ferrite in a low-carbon steel. Metall Mater Trans A 2006;37:609–19.

[14] Threadgill PL, Leonard AJ, Shercliff HR, Withers PJ. Friction stir welding of aluminium alloys. Int Mater Rev 2009;54:49–93.

[15] Svensson L-E, Karlsson L, Larsson H, Karlsson B, Fazzini M, Karlsson J. Microstructure and mechanical properties of friction stir welded aluminium alloys with special reference to AA 5083 and AA 6082. Sci Technol Weld Join 2000;5:285–96.

[16] Janjić M, Vukčević M, Mandić V, Pavletić D, Šibalić N. Microstructural evolution during friction stir welding of AlSi1MgMn alloy. Metalurgija 2012;51:29–33.

[17] British Standards Institution. Aluminium and aluminium alloys - Sheet, strip and plate - Part 2. BS EN 485-2. London; 2013.

[18] Adamowski J, Szkodo M. Friction Stir Welds (FSW) of aluminium alloy AW6082-T6. J Achiev Mater Manuf Eng 2007;20:403–6.

[19] Kou S. Welding metallurgy. 2nd ed. New Jersey: Wiley-Interscience; 1987.

[20] Toumpis A, Galloway A, Cater S, McPherson N. Development of a Process Envelope for Friction Stir Welding of DH36 Steel – A Step Change. Mater Des 2014;62:64-75.

**Figure Captions**

Figure 1 – *Schematics showing: (a) conventional rotating shoulder, (b) stationary shoulder friction stir welding techniques. Image reproduced with permission from TWI*

Figure 2 – *Machined specimen for bend/crush testing of the T-joints, produced using the stationary shoulder FSW technique. Note that the leg and base of the specimen have been reduced to equal length and force was applied such that the face of the weld was put subject to tensile bending stress.*

Figure 3 – *Macrographs showing friction stir butt welds produced in DH36 steel using different tool rotation and traverse speeds: (a) W1 at 200rpm and 120mm/min, (b) W2 at 200rpm and 140mm/min, (c) W3 at 200rpm and 160mm/min, (d) W4 at 600rpm and 450mm/min*

Figure 4 – *Light microscopy imaging regions utilised for all of the DH36 specimens.*

Figure 5 – *Micrographs showing variation in resultant microstructure through the thickness, all micrographs were taken from W2: (a) Region 2 of Figure 4, (b) Region 5 of Figure 4, (c) Region 8 of Figure 4.*

Figure 6 – *Micrograph showing region 5 of Figure 4 in W4. Note the predominant bainitic ferrite phase as a result of the FSW process parameters utilised.*

Figure 7 – *Micrograph showing variation of HAZ width with differing FSW parameters: (a) Region 6 of W1, (b) Region 6 of W2, (c) Region 6 of W3*

Figure 8 – *Micrograph showing region 9 of Figure 4 in W3, the 'swept up' type feature on the advancing side which was present in all of the DH36 friction stir welds. This is likely the result of the tool geometry and the movement of plasticised material from the advancing to the retreating side of the weld.*

Figure 9 – *Micrograph showing region 5 of Figure 4 in W3, the centreline segregation of the plate has been swept into the centre of the weld during the FSW process and may be seen as 'swirled' in the resultant microstructure. This swirling is likely due to the tool geometry and more specifically the threading present on the pin of the FSW tool.*

Figure 10 – *Microhardness mapping results for friction stir welds produced in DH36 steel: (a) W1, (b) W2, (c) W3, (d) W4*

Figure 11 – *Macrograph of 6082-T6 aluminium friction stir welds: (a) butt joint produced using conventional FSW techniques, (b) T-joint produced using the stationary shoulder FSW technique.*

Figure 12 – *Light microscopy imaging regions utilised for the aluminium friction stir welds: (a) butt joint, (b) T-joint*

Figure 13 – *Micrographs showing region 3 transition between parent and stirred material: (a) butt joint produced with conventional rotating shoulder FSW tool, (b) T-joint produced using SSFSW*

Figure 14 – *Micrograph showing region 6 of Figure 12(b). The swirling patterns evident on the macrograph of 11(b) are presented, note the use of polarising light and differential interference contrast to highlight the slight topography associated with slight features.*

Figure 15 – *Micrograph showing region 7 of Figure 12(a). Some swirling similar to that observed in the T-joint is shown, in addition, the darker stringer on the right hand side of the micrograph may be traced from the surface of the weld and thus is likely oxide or surface contaminant swept through the welded material.*

Figure 16 – *Microhardness mapping results for the friction stir welds produced in 6082-T6 aluminium: (a) butt joint, (b) T-joint produced using SSFSW technology*

Figure 17 – *All weld metal tensile results for the friction stir welds produced in DH36 steel. The significant increase in yield and tensile strength relative to the parent material of all of the welds is noted. In addition, the significant increase in yield strength of W4 is in conjunction with a low elongation to failure.*

Figure 18 – *Load-extension curves for the aluminium T-joint pull off and pull apart tests. The variation in extension is of note in addition to the approximately equal values of ultimate load prior to failure. The apparent drops in load are the result of the specimens slipping within the grips during testing.*

Figure 19 – *Macrograph showing the weld face following bend testing. 3 cracks are observed and annotated on the surface.*

Figure 1



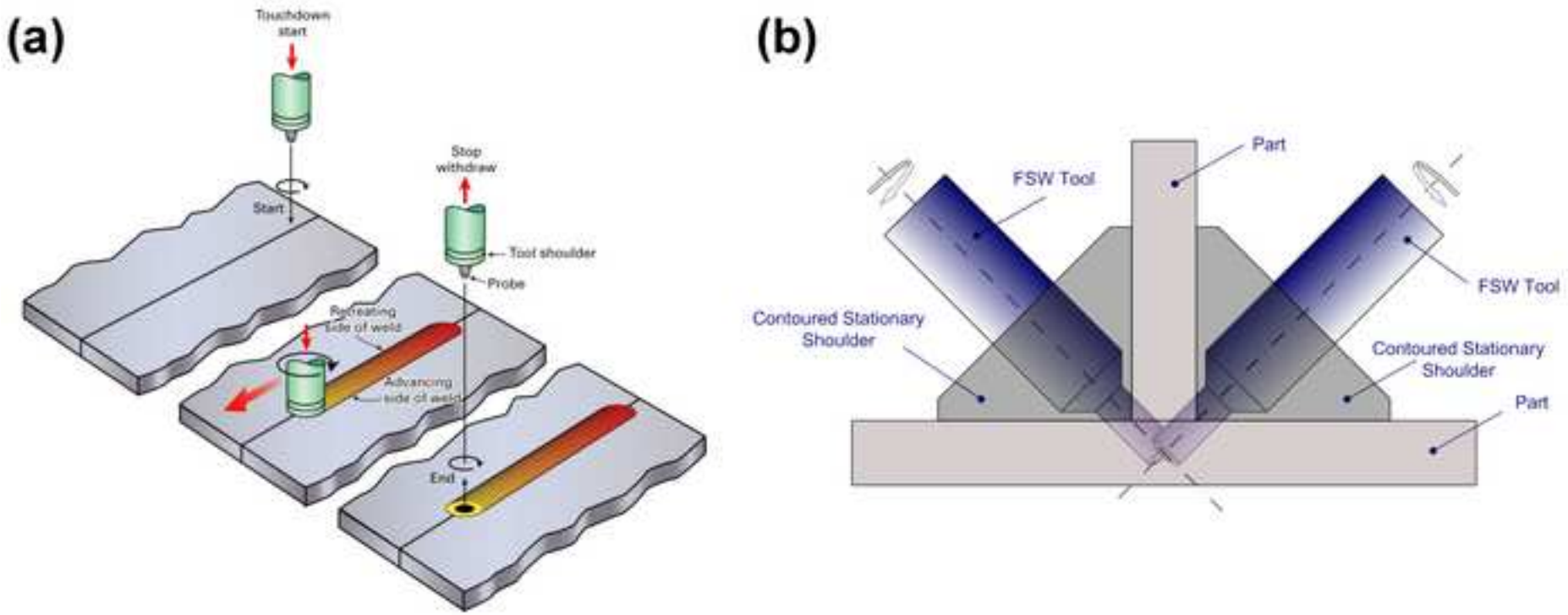

Figure 2



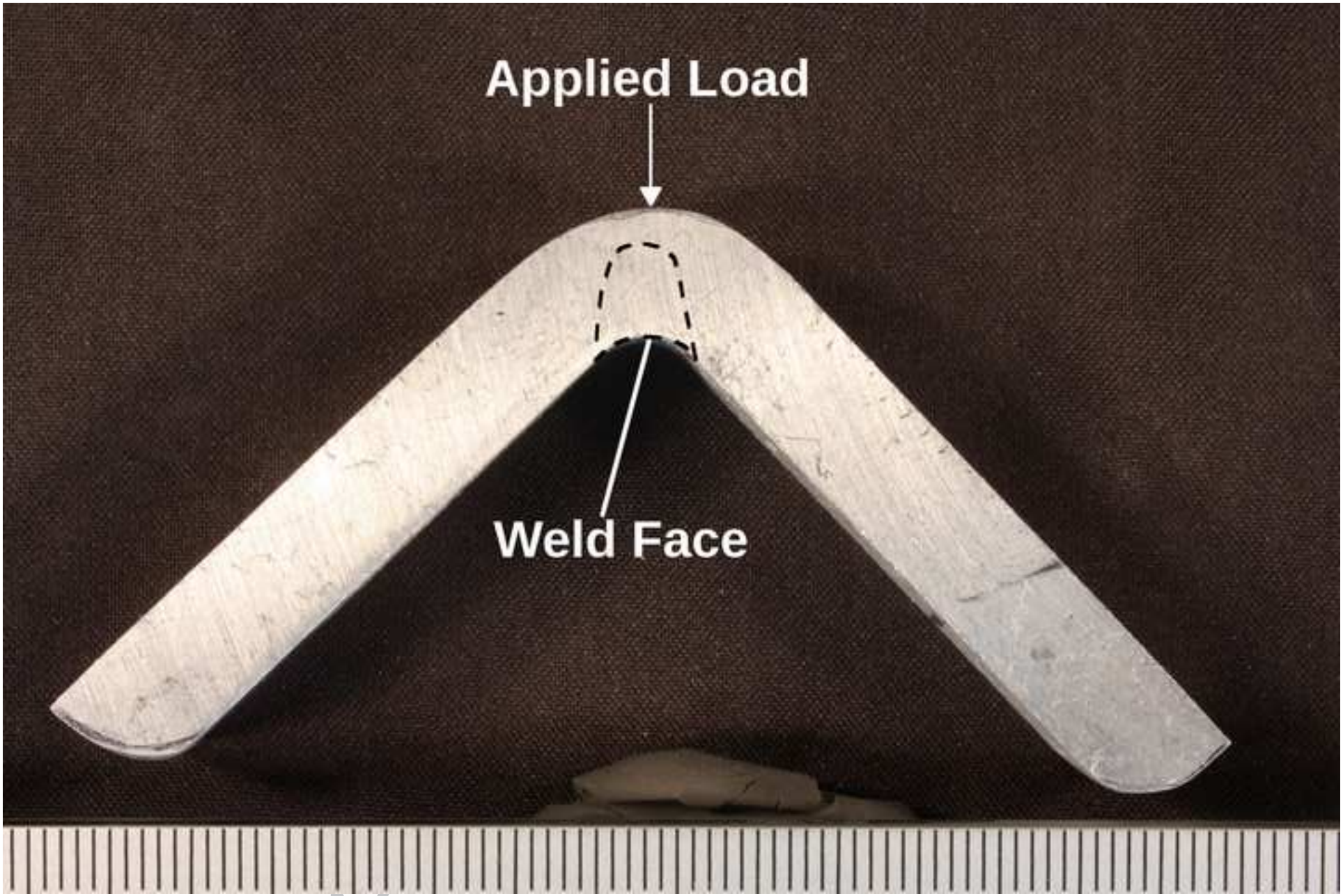

Figure 3



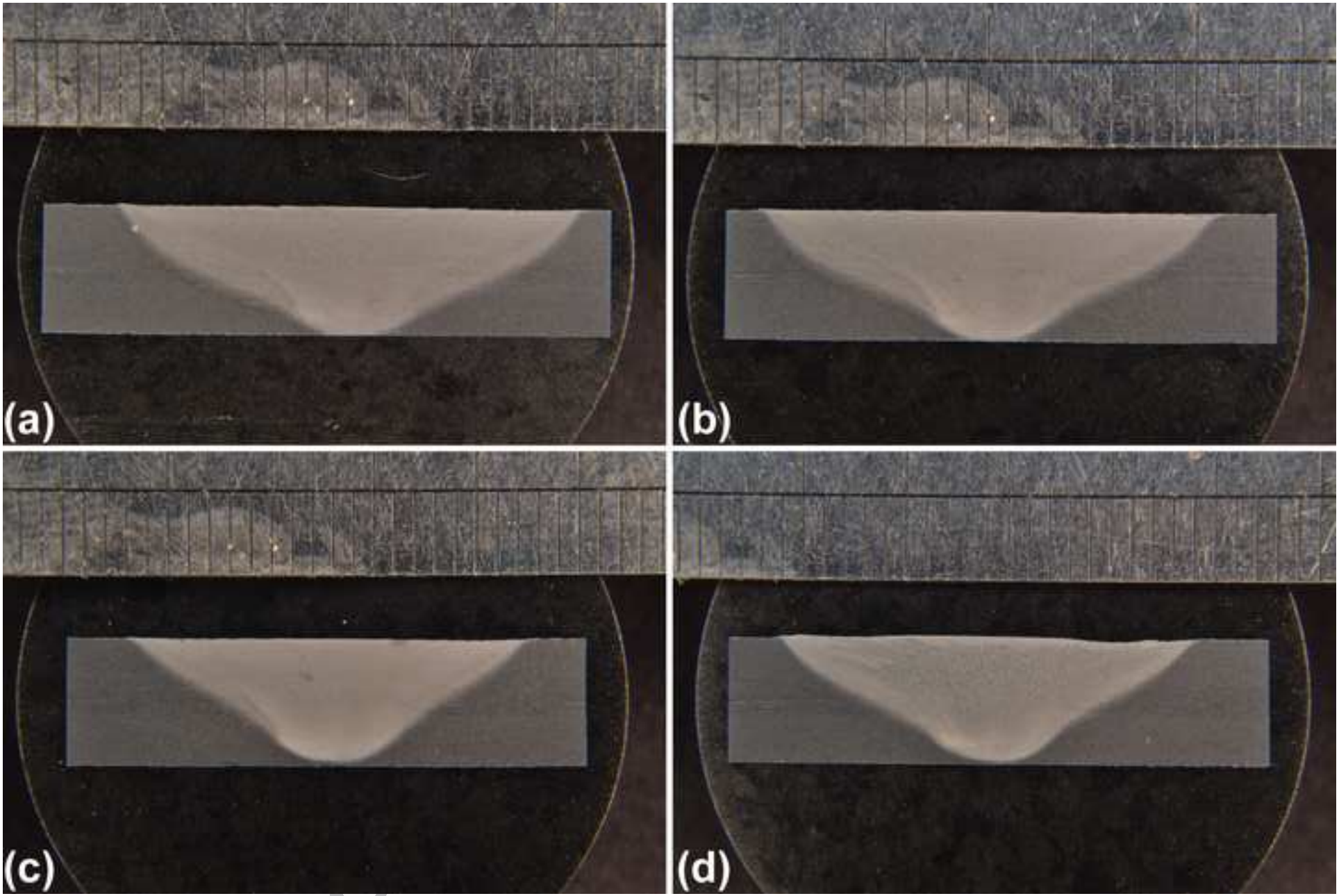

Figure 4



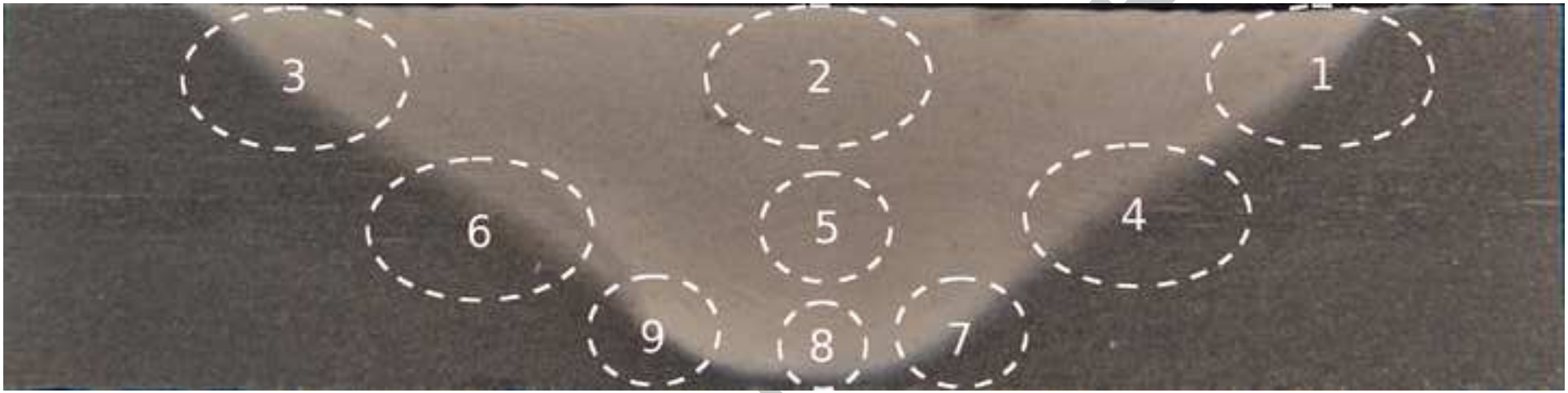

Figure 5



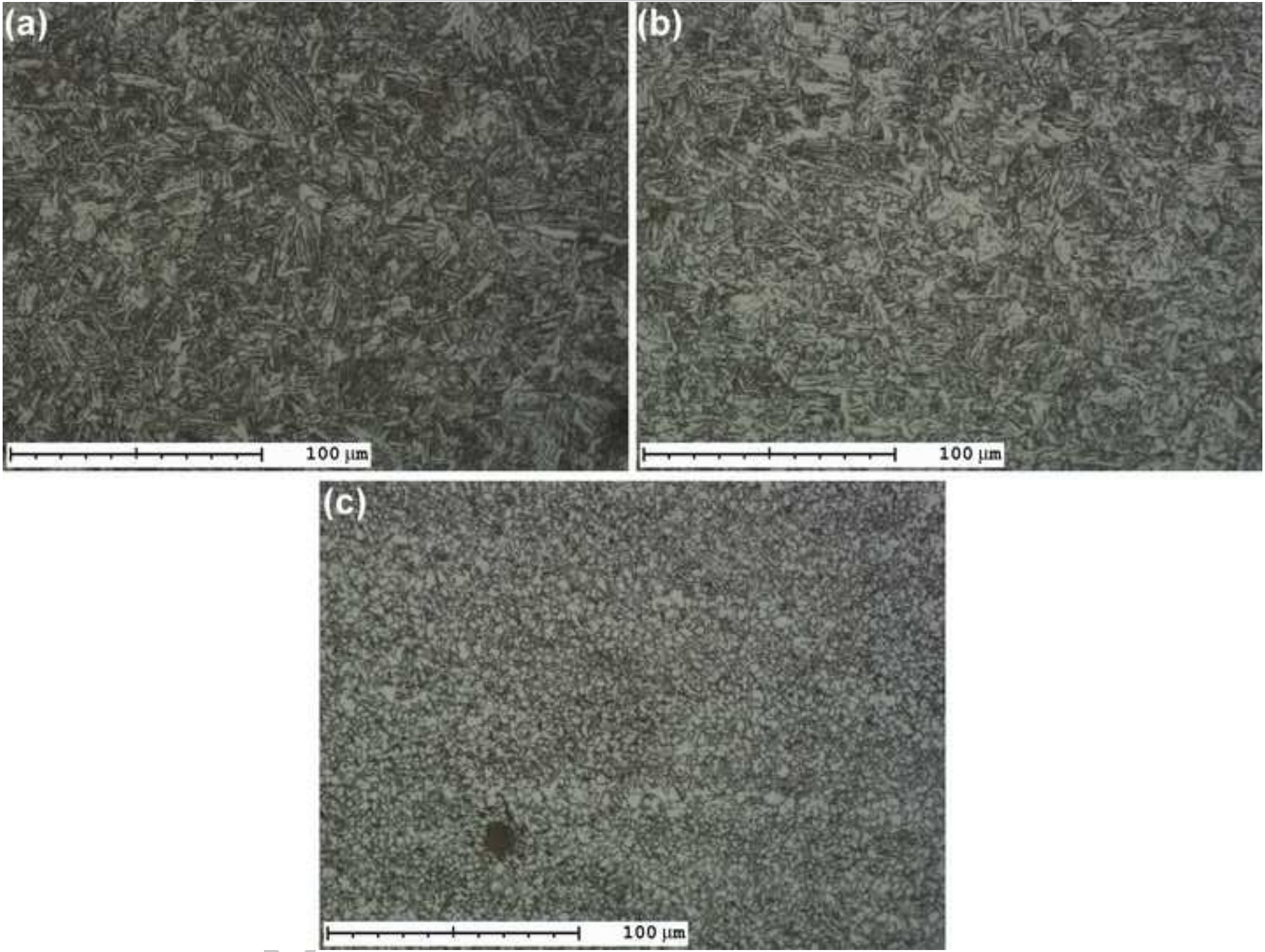

Figure 6



Figure 7



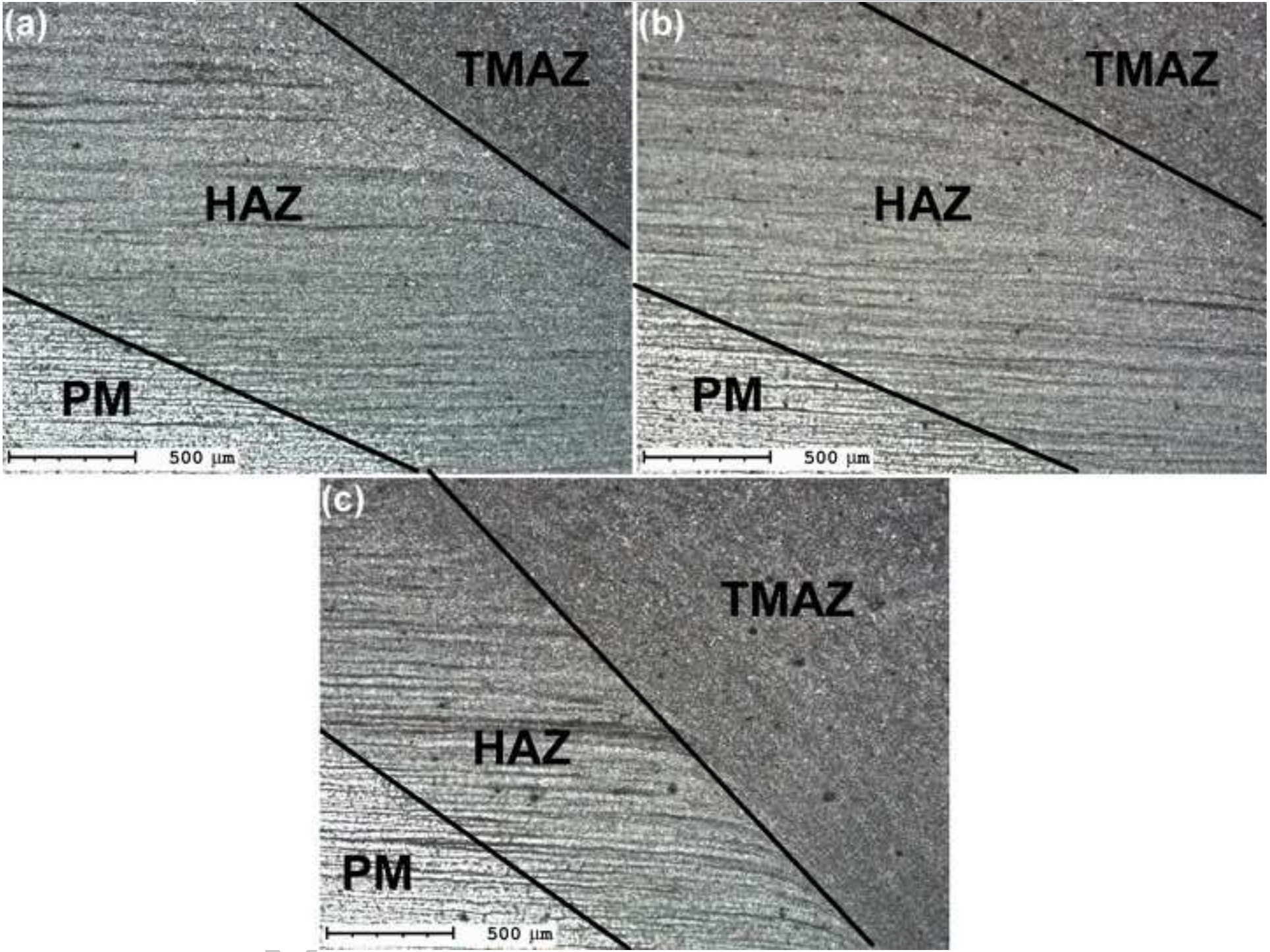

Figure 8



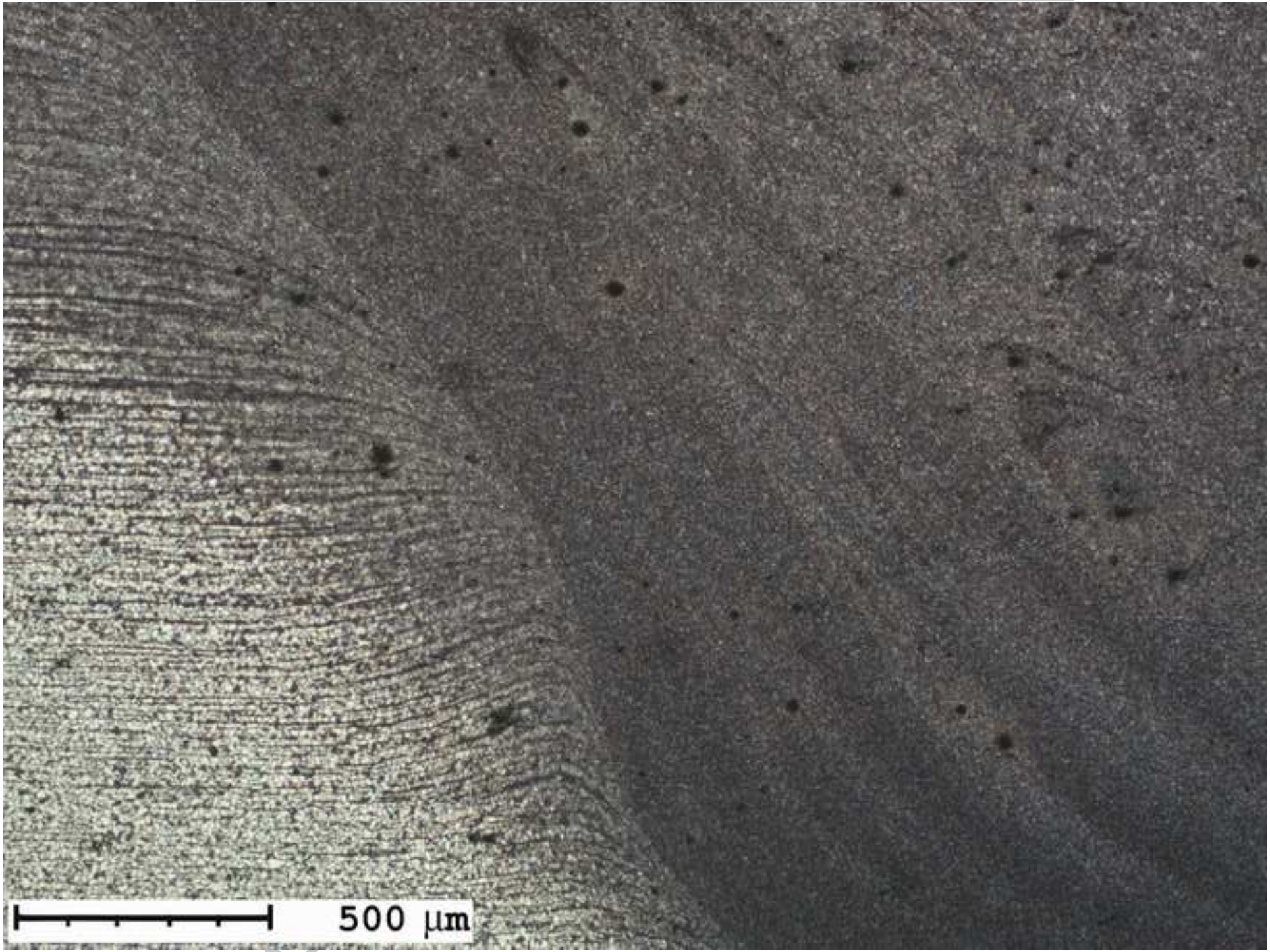

Figure 9



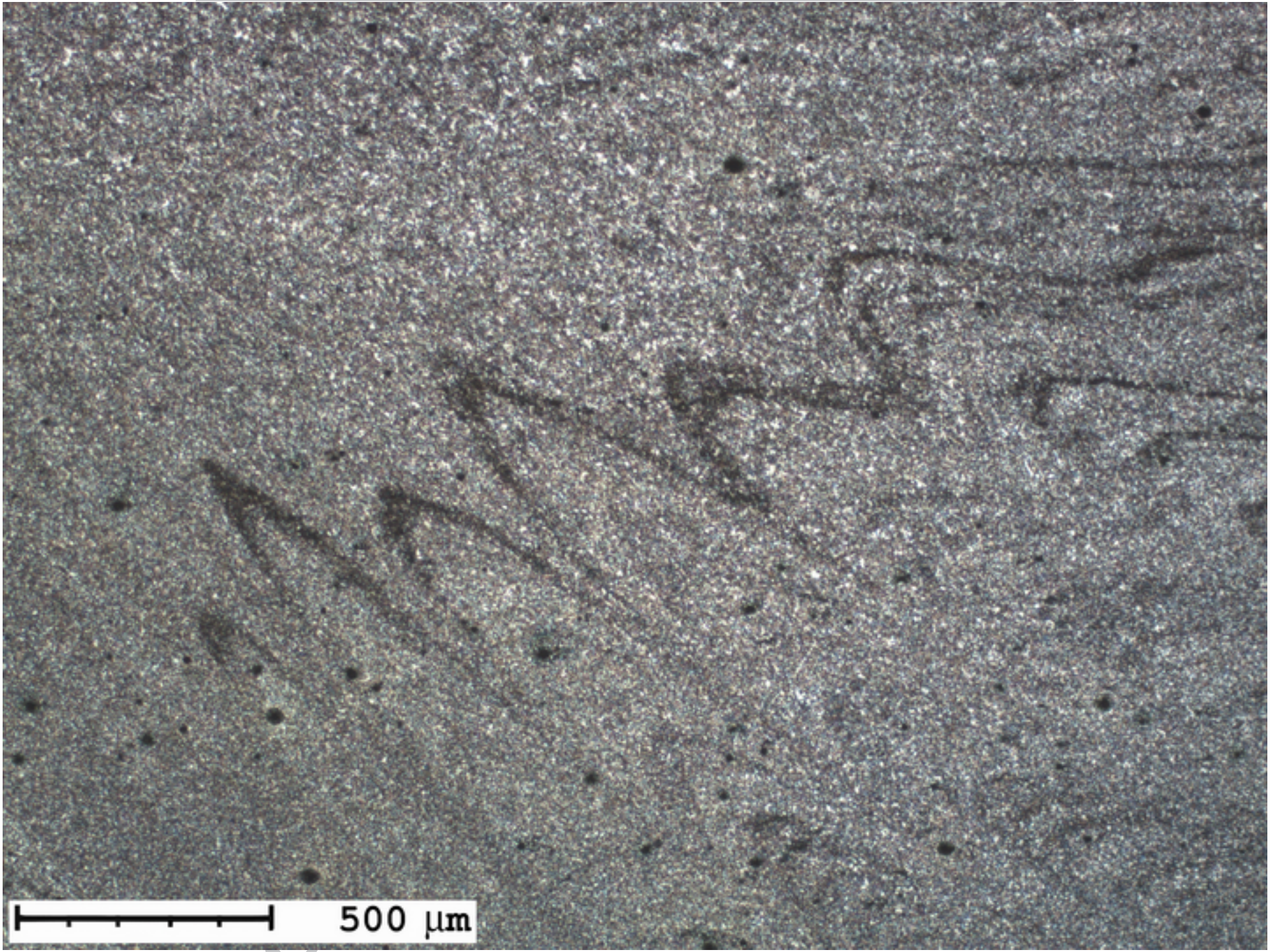

Figure 10



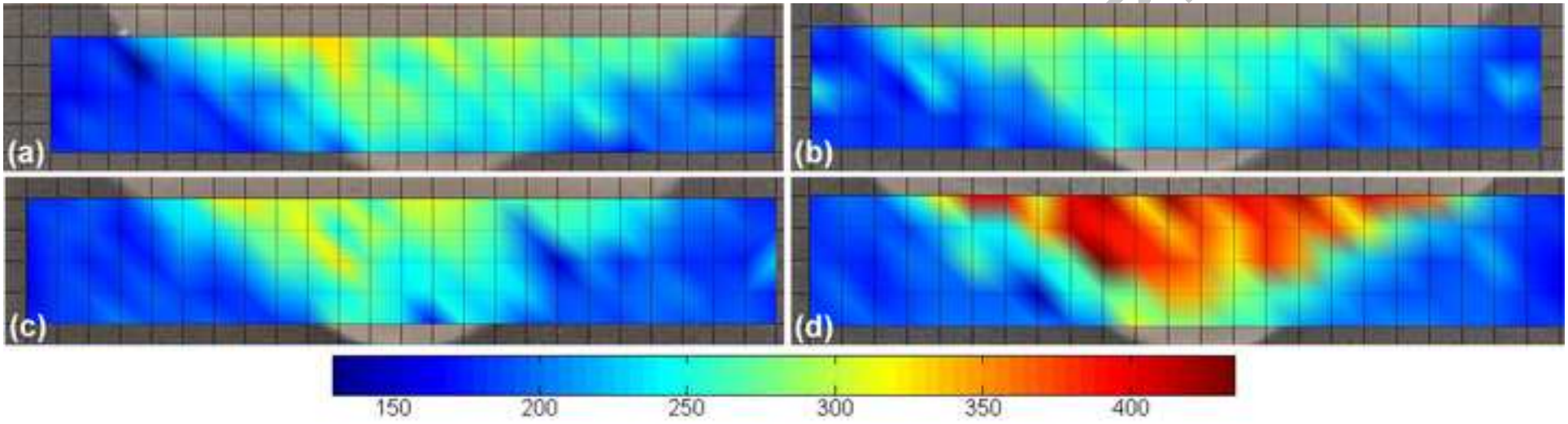

Figure 11



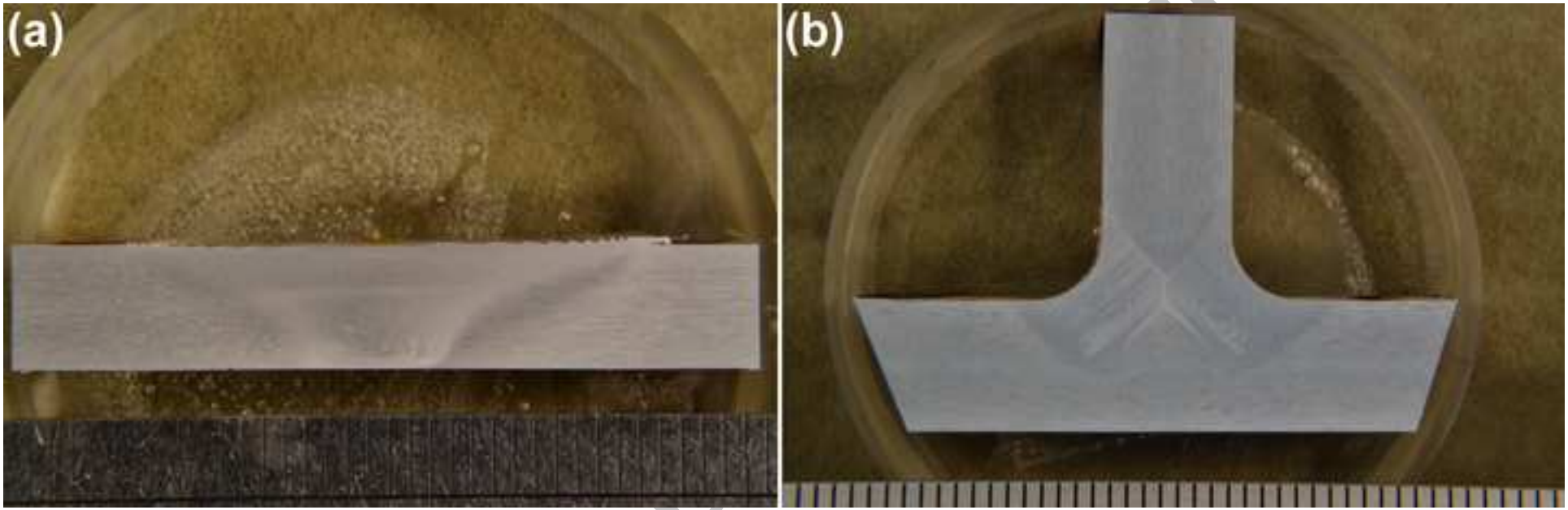

Figure 12



Figure 13



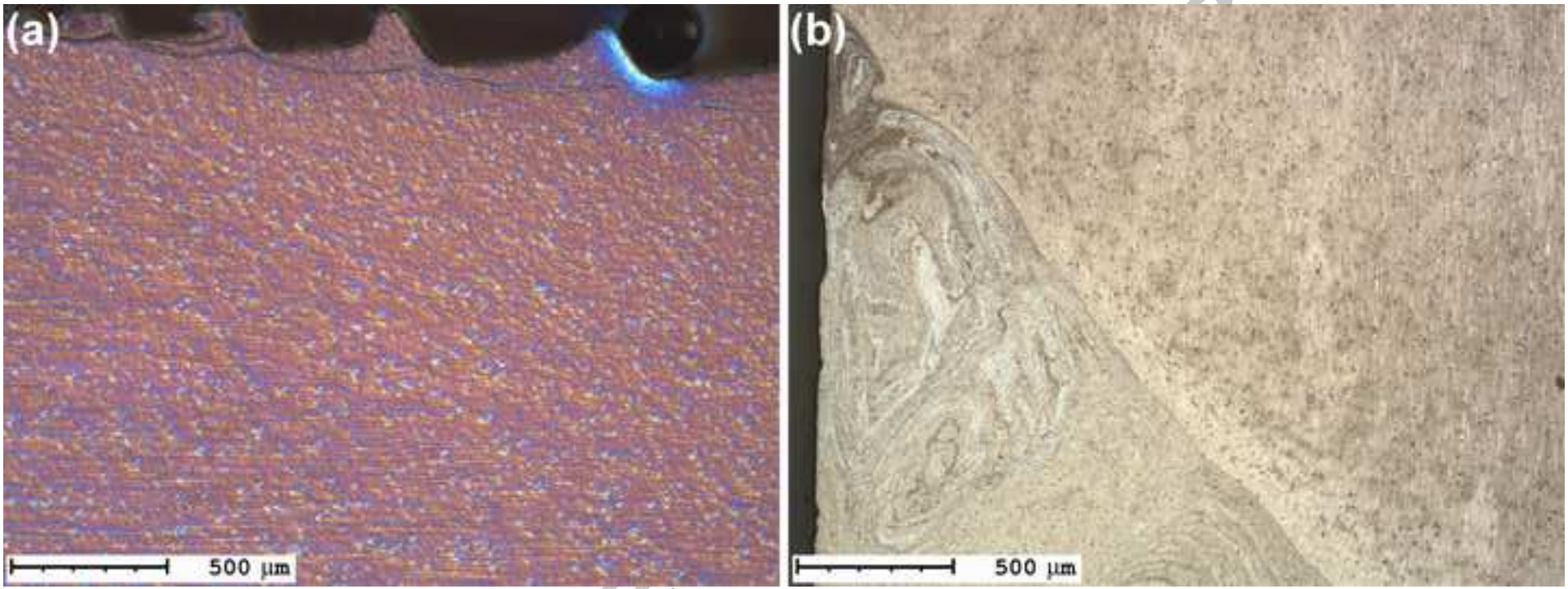

Figure 14



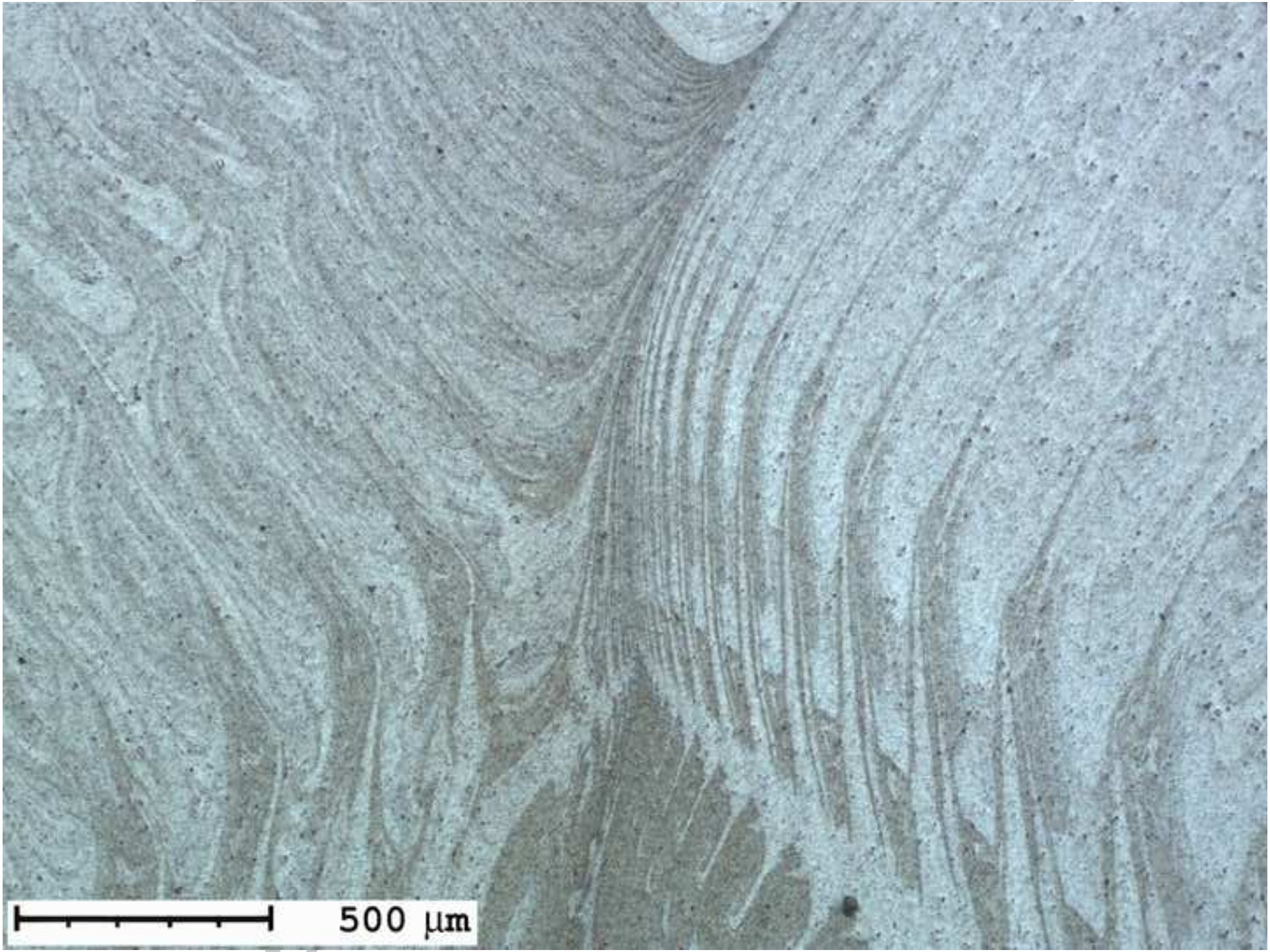

Figure 15



Figure 16



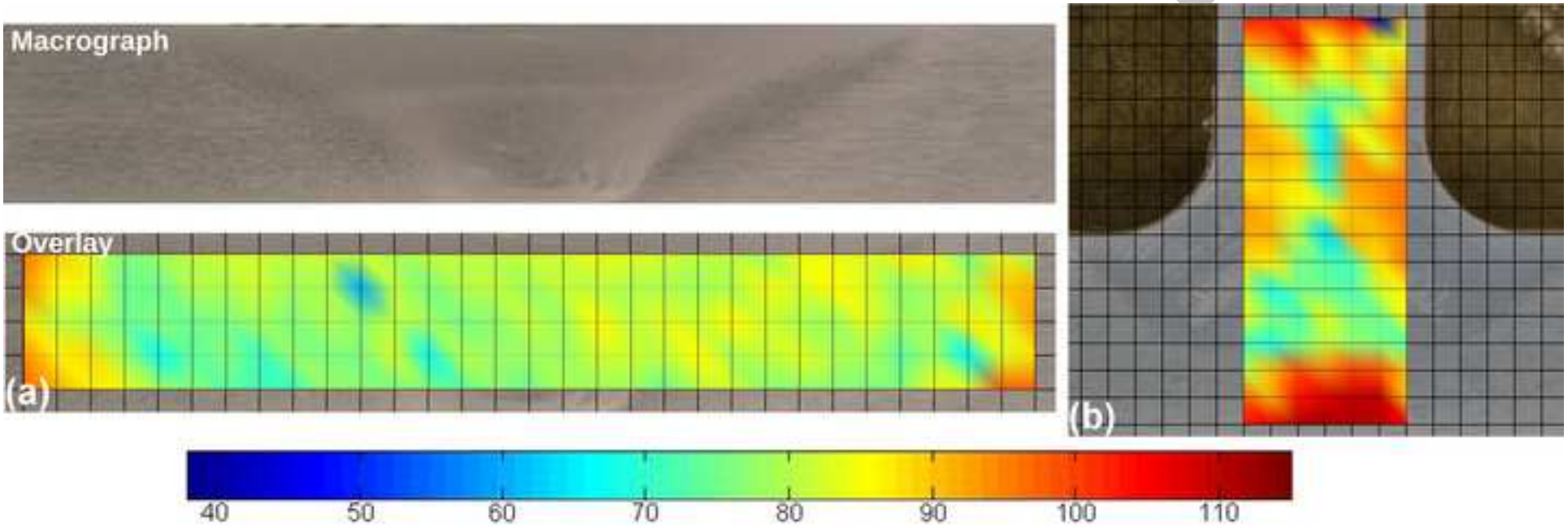

Figure 17



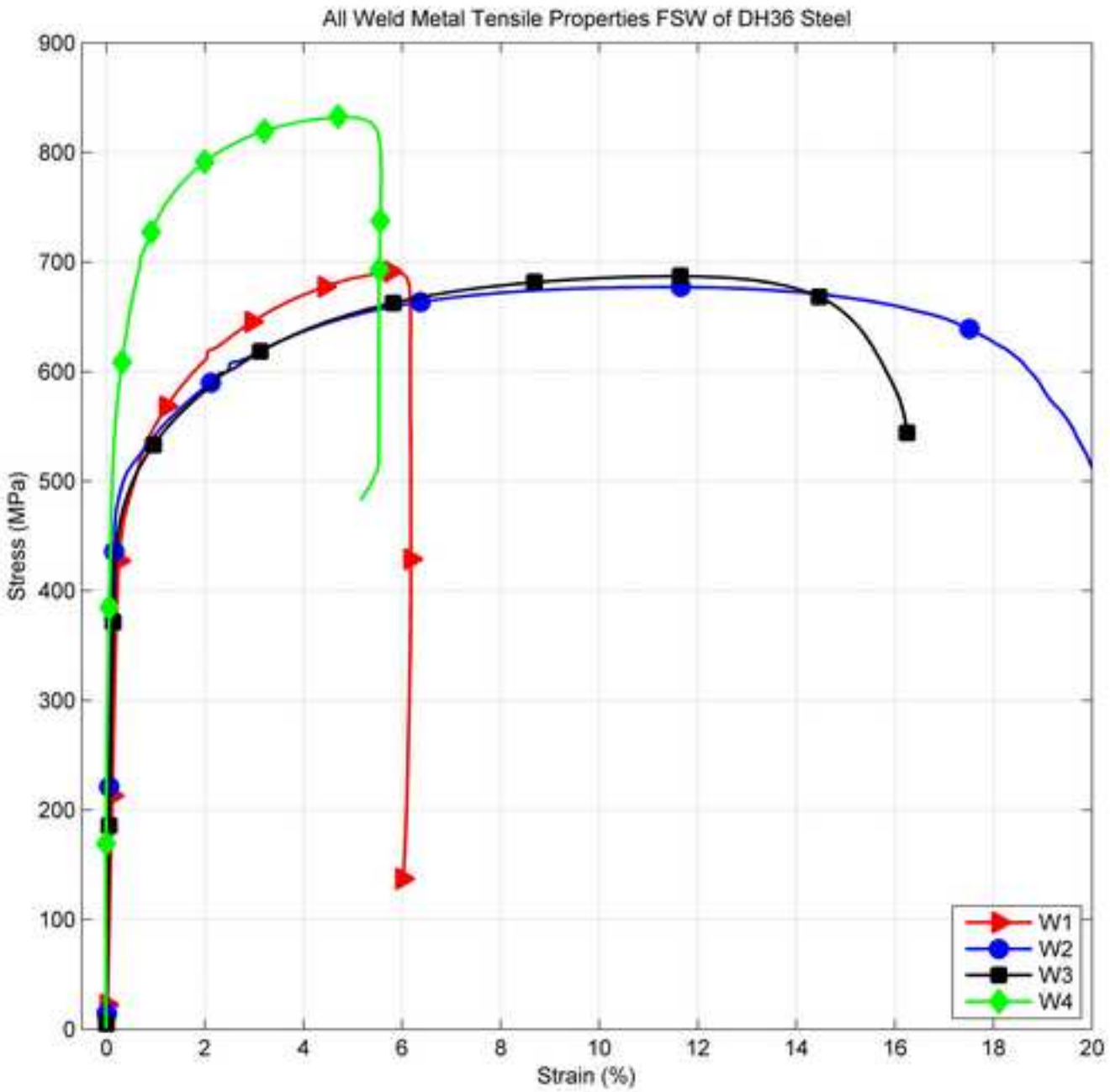

Figure 18



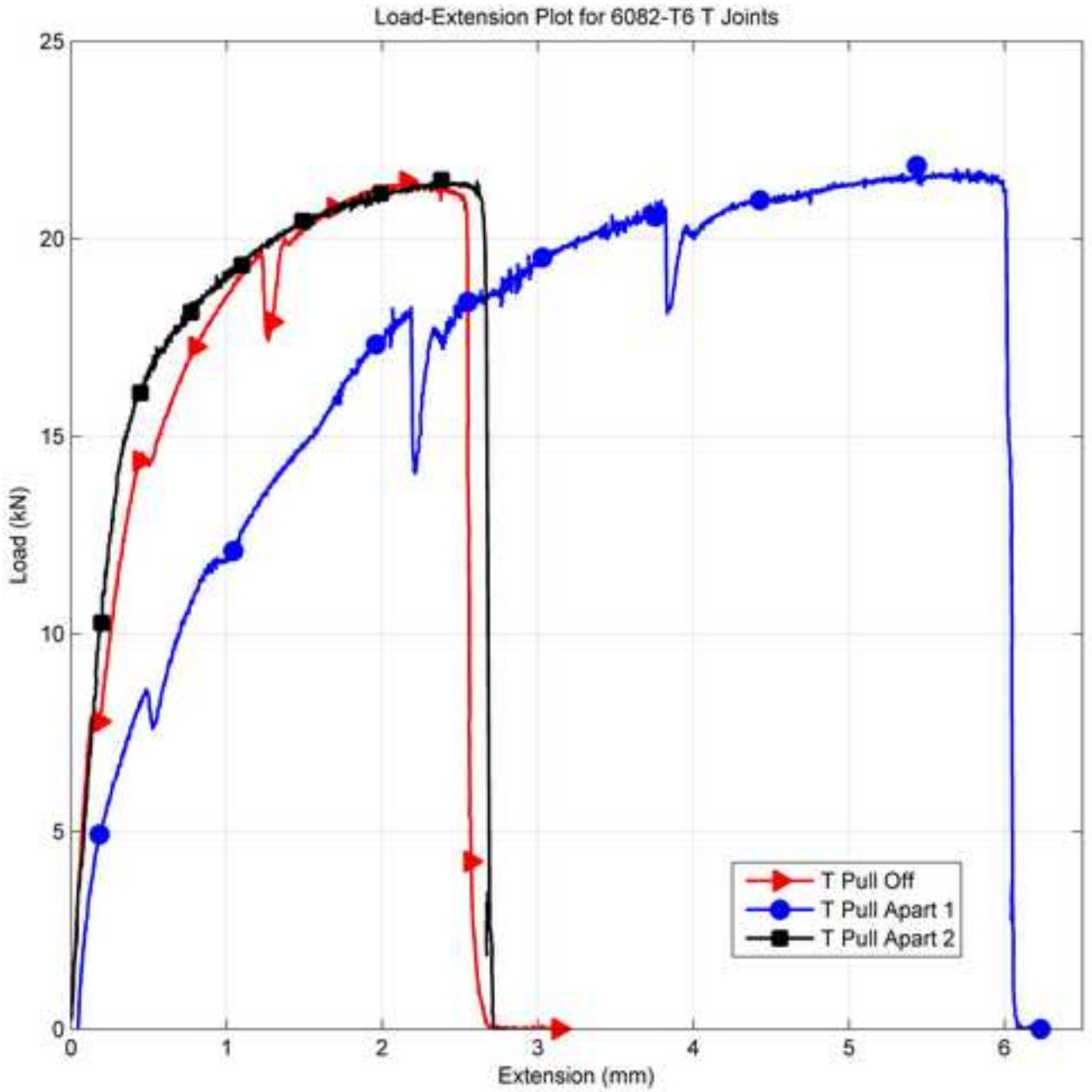

Figure 19



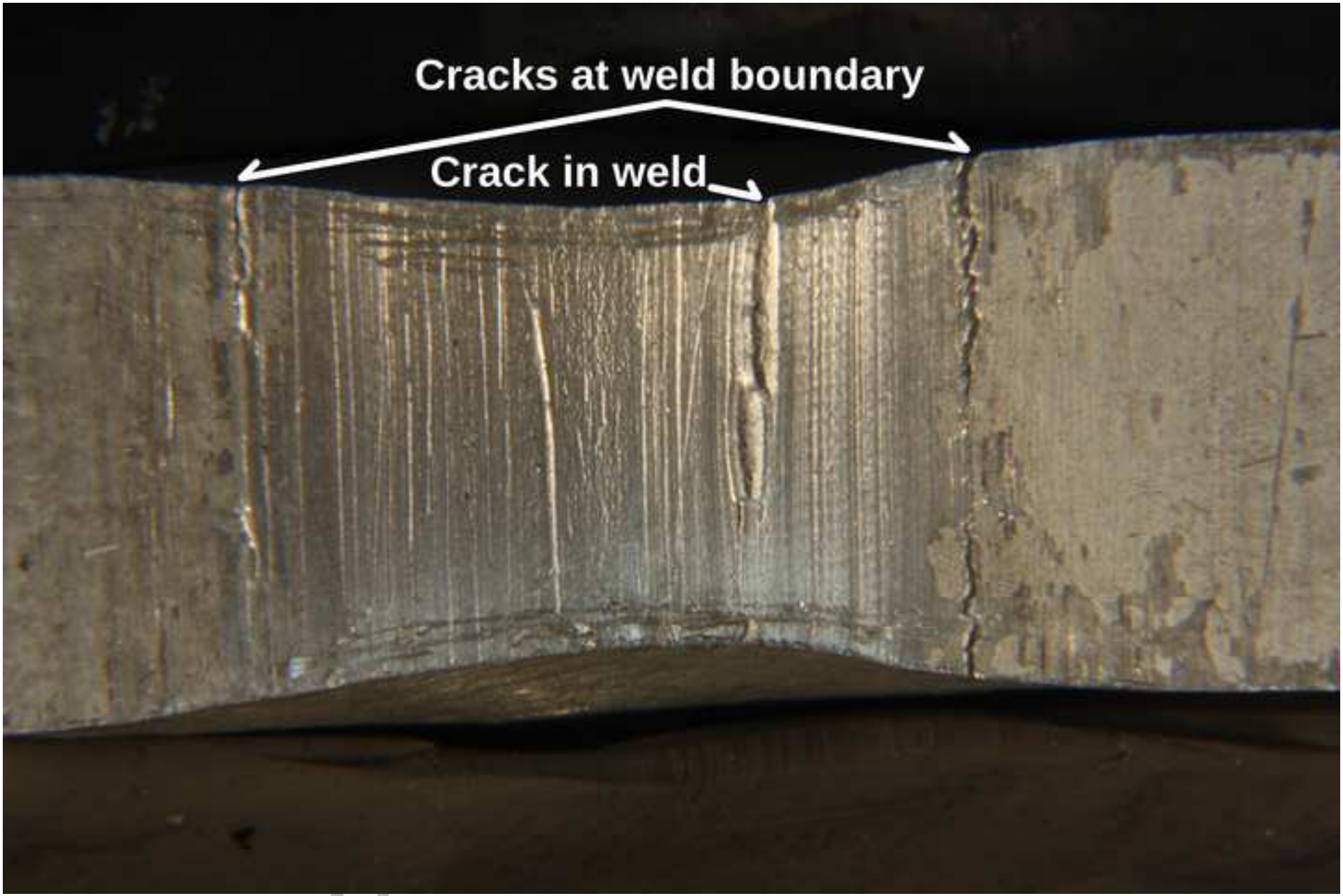

**Tables**

| *C* | *Mn* | *Si* | *P* | *S* | *Al* | *Cb* | *V* | *Ti* | *Cu* | *Cr* | *Ni* | *Mo* |
|---|---|---|---|---|---|---|---|---|---|---|---|---|
| 0.18 max | 0.9-1.6 | 0.1-0.5 | 0.035 max | 0.035 max | 0.015 max | 0.02-0.05 | 0.05-0.10 | 0.02 max | 0.35 max | 0.2 max | 0.4 max | 0.08 max |

***Table 1: DH36 Steel nominal chemical composition values are in maximum wt-% unless otherwise stated***

| *Weld Designation Number* | *Tool Rotation Speed (rpm)* | *Tool Traverse Speed (mm/min)* |
|---|---|---|
| W1 | 200 | 120 |
| W2 | 200 | 140 |
| W3 | 200 | 160 |
| W4 | 600 | 450 |

***Table 2: Steel weld designation and welding parameters***

| *Al* | *Si* | *Fe* | *Cu* | *Mn* | *Mg* | *Cr* | *Zn* | *Ti* | *Others* | |
|---|---|---|---|---|---|---|---|---|---|---|
| | | | | | | | | | *Each* | *Total* |
| Bal | 0.7-1.3 | 0.5 max | 0.1 max | 0.4-1.0 | 0.6-1.2 | 0.25 max | 0.2 max | 0.1 max | 0.05 | 0.15 |

***Table 3: 6082-T6 Aluminium nominal chemical composition are in maximum wt-% unless otherwise stated***

| *Weld Designation* | *Parent Material* | | *Transverse Tensile* | | *All Weld Metal Tensile* | |
|---|---|---|---|---|---|---|
| | **0.2%PS (MPa)** | **UTS (MPa)** | **0.2%PS (MPa)** | **UTS (MPa)** | **0.2%PS (MPa)** | **UTS (MPa)** |
| W1 | 387.01 | 540.53 | 383.67 | 550.16 | 482.16 | 691.24 |
| W2 | 374.34 | 530.24 | 360.27 | 547.36 | 503.01 | 672.48 |
| W3 | 380.79 | 534.95 | 371.97 | 544.48 | 481.93 | 687.37 |
| W4 | 376.71 | 531.62 | 360.76 | 536.46 | 656.68 | 832.51 |

***Table 4: Tensile properties of friction stir welded DH36***

| Weld Designation | Dimensions (mm) | Absorbed Energy (J) | Average (J) | ρ ($J/cm^2$) |
|---|---|---|---|---|
| W1 | 5x10x2V | 69; 56; 61 | 62.00 | 155 |
| W2 | 5x10x2V | 50; 52; 49.5 | 50.50 | 126.25 |
| W3 | 5x10x2V | 46.5; 50; 59 | 51.83 | 129.58 |
| W4 | 5x10x2V | 46; 32.5; 36 | 38.17 | 95.43 |

***Table 5: Charpy V-notch impact properties of friction stir welded DH36***

| Plate Location | 0.2% PS (MPa) | 0.5% RT (MPa) | UTS (MPa) |
|---|---|---|---|
| End | 152.39 | 157.47 | 257.71 |
| Middle | 149.50 | 154.86 | 250.18 |

***Table 6: Tensile properties of friction stir welded 6082-T6 aluminium***

| Notch Location | Dimensions | Energy Absorbed (Joules) | Average (Joules) | ρ ($J/cm^2$) |
|---|---|---|---|---|
| Weld centreline | 5x10x2V | 20; 22; 20.5 | 20.83 | 52.08 |

***Table 7: Charpy V-notch impact properties of friction stir welded 6082-T6 aluminium***

**Highlights**

- The potential transfer of stationary shoulder FSW to steel has been investigated
- Al SSFSW has shown a distinct boundary between stirred and unstirred material
- DH36 butt welds have shown increases in strength but reduction in toughness
- If this abrupt transition occurred in steel, it could cause crack initiation